Flexible Batteries

Deutsche Ausgabe: DOI: 10.1002/ange.201601804
Internationale Ausgabe: DOI: 10.1002/anie.201601804

An All-Solid-State Fiber-Shaped Aluminum–Air Battery with Flexibility, Stretchability, and High Electrochemical Performance

*Yifan Xu[+], Yang Zhao[+], Jing Ren, Ye Zhang, and Huisheng Peng**

Abstract: *Owing to the high theoretical energy density of metal–air batteries, the aluminum–air battery has been proposed as a promising long-term power supply for electronics. However, the available energy density from the aluminum–air battery is far from that anticipated and is limited by current electrode materials. Herein we described the creation of a new family of all-solid-state fiber-shaped aluminum–air batteries with a specific capacity of 935 mAh g^{-1} and an energy density of 1168 Wh kg^{-1}. The synthesis of an electrode composed of cross-stacked aligned carbon-nanotube/silver-nanoparticle sheets contributes to the remarkable electrochemical performance. The fiber shape also provides the aluminum–air batteries with unique advantages; for example, they are flexible and stretchable and can be woven into a variety of textiles for large-scale applications.*

The global requirement for high-performance energy devices has been increasing rapidly.[1–5] Metal–air batteries have been widely studied as the next-generation power systems owing to their environmental friendliness, low cost, and potential high energy-storage capability.[6] For example, the active material in the cathode is the oxygen in air, which leads to a higher theoretical energy density as compared to that of traditional batteries (e.g., lithium-ion battery).[7] More specifically, the aluminum–air (Al–air) battery reveals a theoretical energy density of 2796 Wh kg^{-1}, which is over ten times that of the commercial lithium-ion battery.[8] However, the expected high energy density does not occur in the current Al–air battery.

The electrochemical performance is mainly limited by the air cathode.[9–12] Oxygen is reduced at the triple phase boundary of the air cathode in contact with the electrolyte and air during discharging. The major obstacles are the slow oxygen diffusion and sluggish oxygen-reduction reaction (ORR) without catalysis in the air electrode.[8] Therefore, a lot of effort has been made to design the air cathode with a three-dimensional porous framework, which may promote oxygen diffusion through the gas phase and enhance the ORR catalytic activity.[13–17] Furthermore, conventional Al–air batteries typically appear as a rigid bulk structure enabled by the current air electrodes,[18,19] which cannot meet the required flexibility and stretchability in the next-generation flexible and wearable electronics.

In this study, a new fiber-shaped Al–air battery (Figure 1) was neatly made by sequentially coating a gel electrolyte and wrapping cross-stacked carbon-nanotube (CNT)/silver-nanoparticle hybrid sheets as the air cathode onto a springlike Al substrate (see Figure S1 in the Supporting Information). This

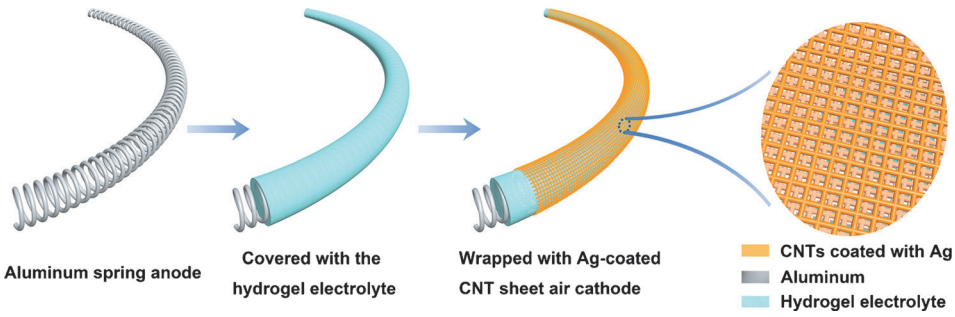

Figure 1. Fabrication of the fiber-shaped Al–air battery.

design offers four promising advantages: 1) The aligned and cross-stacked CNT sheets produce a porous framework to effectively adsorb oxygen, and the deposited Ag nanoparticles serve as a high-efficiency catalyst to significantly enhance the energy-storage capability. 2) The modified hydrogel electrolyte decreases the corrosion of the Al spring and increases their stability and safety. 3) The CNT sheet, hydrogel electrolyte, and Al spring are flexible and stretchable, which provides the resulting Al–air battery with flexibility and stretchability. 4) The fiber shape enables some interesting properties, for example, these Al–air batteries can be woven into self-powered textiles to create various flexible and wearable electronic devices.

Aligned CNT sheets proved to be suitable as the air cathode because of their high electrical conductivity and tensile strength.[20–22] To prepare the air cathode, aligned CNT sheets drawn from a spinnable CNT array were first cross-stacked layer by layer onto a Teflon plate. The building CNTs remained highly aligned and formed a porous structure (see Figure S2), so oxygen could be effectively adsorbed and

[*] Y. Xu,[+] Y. Zhao,[+] J. Ren, Y. Zhang, Prof. Dr. H. Peng
State Key Laboratory of Molecular Engineering of Polymers
Collaborative Innovation Center of Polymers and Polymer Composite Materials, Department of Macromolecular Science and Laboratory of Advanced Materials, Fudan University, Shanghai 200438 (China)
E-mail: penghs@fudan.edu.cn

[+] These authors contributed equally to this work.

Supporting information for this article can be found under: http://dx.doi.org/10.1002/anie.201601804.

diffused through the air cathode. However, pristine CNTs showed low catalytic activity in the ORR in aqueous solution.[7] Therefore, the aligned CNTs were further coated with Ag nanoparticles to improve their catalytic properties. It was expected that during the discharging process, oxygen would be reduced to OH^- at the air cathode, and the deposited Ag nanoparticles could catalyze the ORR process.[23] Cyclic voltammograms verified the ORR catalytic ability of CNT/Ag, as an oxygen-reduction peak was observed in an O_2-saturated KOH solution, whereas no peak was found in an N_2-saturated KOH solution (see Figure S3). The silver-coated CNT sheets acted as both a gas-diffusion layer and a current collector, and no additional conductive material or binder was needed in the electrode.

The structure of the air cathode was investigated by scanning electron microscopy (SEM) and transmission electron microscopy (TEM). Figure 2a,b shows typical SEM images of cross-stacked CNT sheets with a Ag load of 45.5 $\mu g\,cm^{-2}$. The aligned structure of the CNTs was well maintained after coating with the Ag nanoparticles, and the Ag nanoparticles were uniformly deposited on their surfaces. A high-resolution TEM image further showed that the surface of a CNT had been fully covered with the Ag nanoparticles as effective ORR sites (Figure 2c). The loading content of Ag nanoparticles could be accurately controlled by varying the coating time, for example, it was found to be 23.3, 45.5, and 66.9 $\mu g\,cm^{-2}$ at 50, 100, and 150 s (Figure 2d–f), respectively. The Ag nanoparticles were effectively coated on the surfaces of aligned CNTs without obvious aggregation (see Figures S4 and S5).

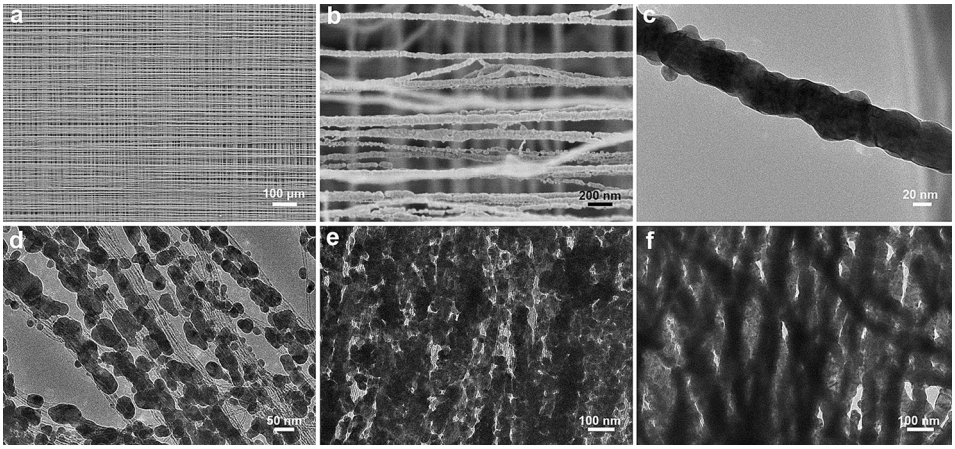

Figure 2. Structural characterization of the air cathode composed of cross-stacked aligned CNT/silver-nanoparticle sheets. a, b) SEM images of cross-stacked CNT sheets with an Ag load of 45.5 $\mu g\,cm^{-2}$ at low and high magnification, respectively. c) TEM image of an silver-coated CNT in (a). d–f) TEM images of cross-stacked CNT sheets with an increasing Ag content of 23.3, 45.5, and 66.9 $\mu g\,cm^{-2}$, respectively.

The electrolyte used in Al-air batteries is typically an aqueous alkaline solution, which readily leads to leakage or a short circuit under bending or stretching. In this study, the hydrogel electrolyte was designed to include poly(vinyl alcohol) (PVA), poly(ethylene oxide) (PEO), and KOH solution with ZnO and Na_2SnO_3 as additives, which not only solved the above problems but also reduced the corrosion of the Al anode in alkaline solution.[24] ZnO served as a corrosion inhibitor of the Al anode. The peak in the polarization curves of Al in the KOH solution after the addition of ZnO indicated the oxidation of Zn deposited on the Al (see Figure S6). Zn was deposited on the Al surface by a replacement reaction after the dissolution of ZnO, and increased the overpotential for hydrogen evolution as a result of the more positive potential of Zn.[24] Na_2SnO_3 decreased the open-circuit potential of Al, which promoted the dissolution of Al in KOH solution. The increase in hydrogen evolution could be countered by the addition of ZnO. Thermodynamically, Al cannot be electrodeposited in aqueous electrolytes; thus, the Al–air battery was not rechargeable.[8] The resulting hydrogel electrolyte could be readily bent or stretched (see Figure S7), and it showed a higher ionic conductivity of 0.18 $S\,cm^{-1}$ (see Figures S8 and S9) as compared to a previously reported solid-state electrolyte.[25] Polymer gel electrolytes commonly show low conductivity, which is attributed to the binding of water by the polymer matrix. In this case, the large amount of free water in the PVA/PEO hydrogel provided the electrolyte with better ion transport.

A fiber-shaped Al–air battery could be then fabricated from the electrode composed of cross-stacked aligned CNT/Ag sheets and a modified gel electrolyte with the Al spring as the substrate (see Figure S10). The impact of the layer number and thickness of the CNT sheets on their electrochemical properties was first investigated. The layer number (N) of cross-stacked hybrid sheets can be calculated by $N=(M\times L)/C$, in which M and L are the number of CNT sheets used and the rolling length on the Teflon plate, respectively; C represents the circumference of the transversal section of the modified spring. The rate discharge performance increased as the layer number increased up to 30, and then decreased a little beyond this point (see Figure S11). As the thickness of an aligned CNT sheet was approximately 20 nm, an air cathode thickness of approximately 600 nm was studied in the following experiments.

The electrochemical performance of the air cathode was further investigated by recording polarization and power-density curves with increasing Ag content (Figure 3a,b). In these experiments, all measurements were conducted in ambient air. The CNT sheets coated with Ag nanoparticles clearly provided better discharge performance than bare CNT sheets without Ag at the same voltage; the current densities of the former were approximately 3–4 times higher than those of the latter. The polarization current densities increased from 1.49 to 1.91 $mA\,cm^{-2}$ as the density of Ag on the surface of the CNT sheets increased from 23.3 to 66.9 $\mu g\,cm^{-2}$ at 0.8 V (Figure 3a). The current density was more obviously enhanced with an increasing amount of Ag below

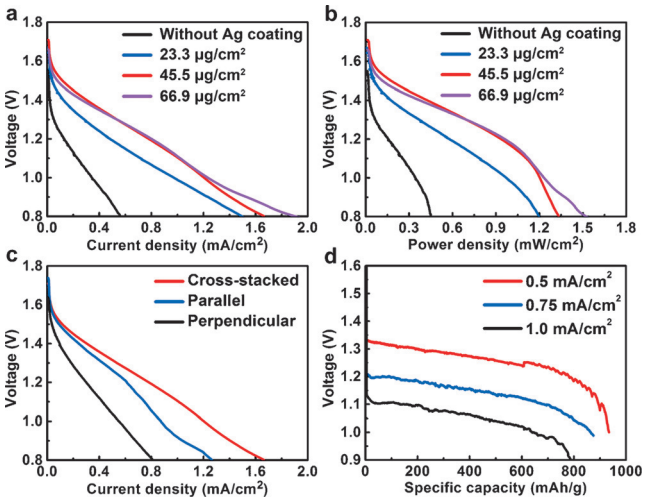

Figure 3. Electrochemical performance of the fiber-shaped Al–air battery. a, b) Polarization and power-density curves of fiber-shaped Al–air batteries with different amounts of Ag on the CNT-sheet air cathode (scan rate: 2 $mV s^{-1}$). c) Polarization curves of fiber-shaped Al–air batteries with CNT/Ag sheet air cathodes in which aligned CNTs were arranged in a cross-stacked pattern or were parallel or perpendicular to the length direction of the fiber battery (scan rate: 2 $mV s^{-1}$). d) Discharge curves of fiber-shaped Al–air batteries at current densities of 0.5, 0.75, and 1.0 $mA cm^{-2}$.

45.5 $\mu g cm^{-2}$, as a certain amount of Ag nanoparticles was needed for the air cathode to effectively catalyze the ORR and to improve the electrical conductivity; the current density was slightly enhanced with increasing Ag at higher contents. The CNT/Ag sheet air cathode before and after discharging was compared by X-ray diffraction spectroscopy (see Figure S12). No Ag_xO was observed after the discharge process,[26] so the Ag functioned as the ORR catalyst. A similar relationship was observed for the power density and Ag content (Figure 3b). Therefore, an Ag load of 45.5 $\mu g cm^{-2}$ was studied in further experiments. The open-circuit potential approached approximately 1.7 V, thus showing the activation of aluminum dissolution.

The porosity of the air cathode was produced by the cross-stacked structure of the CNT sheets, which was crucial to the high electrochemical performance of the fiber-shaped Al–air battery. As control experiments, fiber-shaped Al–air batteries were also fabricated from air cathodes in which aligned CNT sheets were parallel or perpendicular to the length direction of the battery fiber under the same conditions. The polarization current densities were measured as 0.81, 1.26, and 1.66 $mA cm^{-2}$ for the cases in which the aligned CNTs were perpendicular, parallel, and cross-stacked at 0.8 V (Figure 3c). Accordingly, the power densities were calculated as 0.65, 1.01, and 1.33 $mW cm^{-2}$ (see Figure S13). Clearly, the cross-stacked CNT sheets displayed superior rate discharge performance. For the aligned CNTs to be perpendicular or parallel to the battery fiber, the wrapped CNTs contracted, and the smaller pore sizes reduced the adsorption and diffusion of oxygen from the air; in contrast, the formed contacting point between two neighboring crossed CNTs acted as "cross-linking point" to restrict the movement of CNTs in the air cathode (see Figure S14). Therefore, the designed cross-stacked structure offered higher mechanical stability for better electrochemical performance.

For the galvanostatic measurements, the fiber-shaped Al–air battery displayed a specific capacity of 935 $mAh g^{-1}$ based on the consumed aluminum anode (Figure 3d), which is appropriately 6 times higher than that of a fiber-type Zn–C battery.[27] The energy density was calculated as 1168 $Wh kg^{-1}$, which is over 12 times that of a fibrous lithium-ion battery.[28] The maximal power density based on the total volume of the device was calculated as 16.6 $W L^{-1}$, which is over 40 times that of a cable-type Zn–air battery.[29] The specific capacity and maximal power density based on the whole battery were calculated as 12 $Ah kg^{-1}$ and 20 $W kg^{-1}$, respectively. The combined high specific capacity and energy and power densities of the fiber-shaped Al–air battery particularly enable promising applications as a disposable, long-term power supply for miniaturized electronic devices.

The fiber-shaped Al–air battery could be deformed into various shapes and bent to various angles without obvious damage to the structure (see Figure S15). The output voltage remained almost unchanged at a discharge current of 1 mA (Figure 4a). The open-circuit voltage was also maintained by about 98% after bending for 1000 cycles (see Figure S16). A fiber-shaped Al–air battery did not break upon elongation by up to 30%, and the output voltage was also maintained above 1 V during stretching (Figure 4b). Taking into account the movement of the human body, stable discharge under bending and stretching is critical to practical applications. The fiber

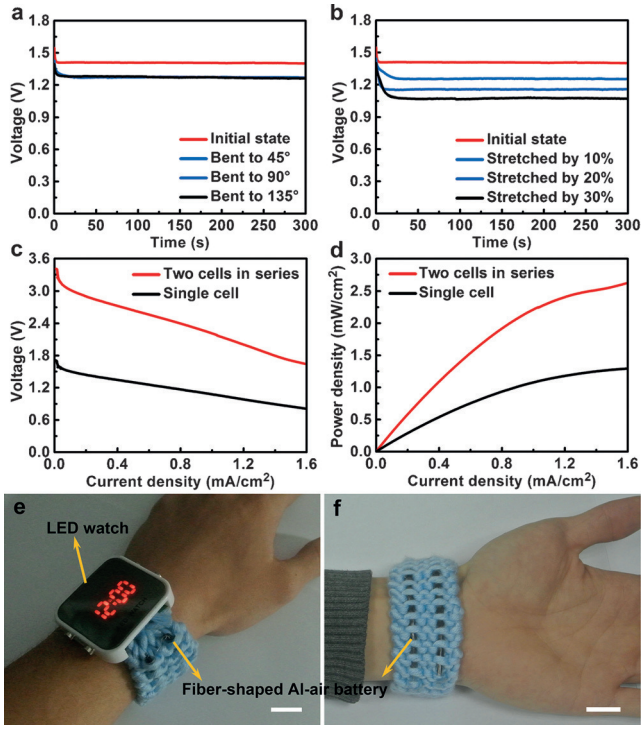

Figure 4. a, b) Discharge curves of fiber-shaped Al–air batteries at different bending angles or stretching ratios at a discharge current of 1 mA. c, d) Polarization and power-density curves of a single fiber-shaped Al–air battery and two batteries in tandem (scan rate: 2 $mV s^{-1}$). e, f) Photographs of a commercial LED watch powered by two fiber-shaped Al–air batteries woven into a fabric and connected in series. Scale bars: 2 cm.

shape makes the battery suitable for being woven into fabrics to create "energetic textiles". As a demonstration, two fiber-shaped Al–air batteries were encapsulated in a porous tube and connected in series to double the output voltage and power (Figure 4c,d); they were woven into a flexible textile to power a light-emitting-diode (LED) watch worn around a human wrist (Figure 4e,f; see also Figure S17).

To summarize, a fiber-shaped all-solid-state Al–air battery has been developed with an air cathode composed of cross-stacked aligned CNT/silver-nanoparticle sheets. The highly porous structure formed by the cross-stacked hybrid sheets promotes gas diffusion, catalyzes the ORR, and enhances electron transport, which enables high electrochemical performance, such as an energy density of 1168 $Wh\,kg^{-1}$. This fiber-shaped Al–air battery is also flexible and stretchable, which may open up new applications in electronics, for example, the powering of smart clothes.

Experimental Section

PVA powder (1 g; molecular weight of 195000, Aladdin) and PEO powder (0.1 g; molecular weight of 100000, Alfa Aesar) were first swollen in deionized water (10 mL) for 5 h and then dissolved at 95 °C under magnetic stirring for 2 h. KOH (1 g), ZnO (0.1 g), and Na_2SnO_3 (0.03 g) were dissolved in deionized water (1 mL), and the supernatant solution was added to the previous polymer solution. The mixture was then kept stirring at 95 °C for 50 min to generate the hydrogel polymer electrolyte solution. An aluminum spring (250 μm in diameter, 99.999 %, Alfa Aesar) with an average pitch of 500 μm was placed in a poly(ethylene terephthalate) tube template (3.2 mm in diameter). The tube template was filled with the hydrogel polymer electrolyte solution and kept in a refrigerator at −20 °C for 1 h to cross-link the electrolyte solution. After freezing, the polymer electrolyte thawed at 4 °C. This cyclic freezing–thawing process was repeated three times to enhance the degree of cross-linking. Finally, the resulting spring was rolled on a Teflon plate covered with the cross-stacked CNT sheets. These CNT sheets were continuously dry-drawn from a CNT array, which was synthesized by chemical vapor deposition,[30] and they were further coated with Ag nanoparticles by vacuum thermal evaporation. The coating time was set at 50, 100, and 150 s with a rate of 5 $Å\,s^{-1}$. A stainless-steel wire was attached to the cathode of the Al–air battery for electrochemical measurements.

Acknowledgments

This research was supported by the NSFC (21225417, 51573027, 51403038), the STCSM (15XD1500400, 15JC1490200), and the Program for Outstanding Young Scholars from the Organization Department of the CPC Central Committee.

Keywords: aluminum–air batteries · carbon nanotubes · electrochemistry · fiber-shaped devices · flexibility

How to cite: *Angew. Chem. Int. Ed.* **2016**, *55*, 7979–7982
Angew. Chem. **2016**, *128*, 8111–8114

[1] T. Chen, R. Hao, H. S. Peng, L. M. Dai, *Angew. Chem. Int. Ed.* **2015**, *54*, 618–622; *Angew. Chem.* **2015**, *127*, 628–632.
[2] M. Armand, J. M. Tarascon, *Nature* **2008**, *451*, 652–657.
[3] P. G. Bruce, S. A. Freunberger, L. J. Hardwick, J. M. Tarascon, *Nat. Mater.* **2012**, *11*, 19–29.
[4] Y. N. Meng, Y. Zhao, C. G. Hu, H. H. Cheng, Y. Hu, Z. P. Zhang, G. Q. Shi, L. T. Qu, *Adv. Mater.* **2013**, *25*, 2326–2331.
[5] X. T. Ding, Y. Zhao, C. G. Hu, Y. Hu, Z. L. Dong, N. Chen, Z. P. Zhang, L. T. Qu, *J. Mater. Chem. A* **2014**, *2*, 12355–12360.
[6] Z. L. Wang, D. Xu, J. J. Xu, X. B. Zhang, *Chem. Soc. Rev.* **2014**, *43*, 7746–7786.
[7] F. Y. Cheng, J. Chen, *Chem. Soc. Rev.* **2012**, *41*, 2172–2192.
[8] Y. G. Li, H. J. Dai, *Chem. Soc. Rev.* **2014**, *43*, 5257–5275.
[9] D. U. Lee, J. Y. Choi, K. Feng, H. W. Park, Z. W. Chen, *Adv. Energy Mater.* **2014**, *4*, 1301389.
[10] Y. C. Lu, B. M. Gallant, D. G. Kwabi, J. R. Harding, R. R. Mitchell, M. S. Whittingham, Y. Shao-Horn, *Energy Environ. Sci.* **2013**, *6*, 750–768.
[11] F. J. Li, T. Zhang, H. S. Zhou, *Energy Environ. Sci.* **2013**, *6*, 1125–1141.
[12] J. T. Zhang, Z. H. Zhao, Z. H. Xia, L. M. Dai, *Nat. Nanotechnol.* **2015**, *10*, 444–452.
[13] H. D. Lim, K. Y. Park, H. Song, E. Y. Jang, H. Gwon, J. Kim, Y. H. Kim, M. D. Lima, R. O. Robles, X. Lepro, R. H. Baughman, K. Kang, *Adv. Mater.* **2013**, *25*, 1348–1352.
[14] T. Y. Ma, J. R. Ran, S. Dai, M. Jaroniec, S. Z. Qiao, *Angew. Chem. Int. Ed.* **2015**, *54*, 4646–4650; *Angew. Chem.* **2015**, *127*, 4729–4733.
[15] H.-D. Lim, H. Song, J. Kim, H. Gwon, Y. Bae, K.-Y. Park, J. Hong, H. Kim, T. Kim, Y. H. Kim, X. Lepró, R. Ovalle-Robles, R. H. Baughman, K. Kang, *Angew. Chem. Int. Ed.* **2014**, *53*, 3926–3931; *Angew. Chem.* **2014**, *126*, 4007–4012.
[16] Y. Xu, Y. Zhang, Z. Guo, J. Ren, Y. Wang, H. Peng, *Angew. Chem. Int. Ed.* **2015**, *54*, 15390–15394; *Angew. Chem.* **2015**, *127*, 15610–15614.
[17] H.-D. Lim, H. Song, H. Gwon, K.-Y. Park, J. Kim, Y. Bae, H. Kim, S.-K. Jung, T. Kim, Y. H. Kim, X. Lepró, R. Ovalle-Robles, R. H. Baughman, K. Kang, *Energy Environ. Sci.* **2013**, *6*, 3570–3575.
[18] D. Gelman, B. Shvartsev, Y. Ein-Eli, *J. Mater. Chem. A* **2014**, *2*, 20237–20242.
[19] L. Wang, F. Liu, W. T. Wang, G. D. Yang, D. W. Zheng, Z. C. Wu, M. K. H. Leung, *RSC Adv.* **2014**, *4*, 30857–30863.
[20] S. Iijima, *Nature* **1991**, *354*, 56–58.
[21] M. F. L. De Volder, S. H. Tawfick, R. H. Baughman, A. J. Hart, *Science* **2013**, *339*, 535–539.
[22] W. Xiong, F. Du, Y. Liu, A. Perez, M. Supp, T. S. Ramakrishnan, L. M. Dai, L. Jiang, *J. Am. Chem. Soc.* **2010**, *132*, 15839–15841.
[23] J. J. Han, N. Li, T. Y. Zhang, *J. Power Sources* **2009**, *193*, 885–889.
[24] D. R. Egan, C. P. de Leon, R. J. K. Wood, R. L. Jones, K. R. Stokes, F. C. Walsh, *J. Power Sources* **2013**, *236*, 293–310.
[25] C. C. Yang, S. J. Lin, *J. Power Sources* **2002**, *112*, 497–503.
[26] X. Y. Gao, S. Y. Wang, J. Li, Y. X. Zheng, R. J. Zhang, P. Zhou, Y. M. Yang, L. Y. Chen, *Thin Solid Films* **2004**, *455*, 438–442.
[27] X. Yu, Y. P. Fu, X. Cai, H. Kafafy, H. W. Wu, M. Peng, S. C. Hou, Z. B. Lv, S. Y. Ye, D. C. Zou, *Nano Energy* **2013**, *2*, 1242–1248.
[28] Y. Zhang, Y. Zhao, X. L. Cheng, W. Weng, J. Ren, X. Fang, Y. S. Jiang, P. N. Chen, Z. T. Zhang, Y. G. Wang, H. S. Peng, *Angew. Chem. Int. Ed.* **2015**, *54*, 11177–11182; *Angew. Chem.* **2015**, *127*, 11329–11334.
[29] J. Park, M. Park, G. Nam, J. Lee, J. Cho, *Adv. Mater.* **2015**, *27*, 1396–1401.
[30] T. Chen, L. B. Qiu, H. G. Kia, Z. B. Yang, H. S. Peng, *Adv. Mater.* **2012**, *24*, 4623–4628.

Received: February 20, 2016
Published online: May 19, 2016

